Vibrational excitation of hydrogen fluoride by low-energy electrons: theory and experiment

M Čížek†, J Horáček†, M Allan‡ I I Fabrikant§ and W Domcke£

† Institute of Theoretical Physics, Faculty of Mathematics and Physics, Charles University Prague, V Holešovičkách 2, 180 00 Praha 8, Czech Republic
‡ Department of Chemistry, University of Fribourg, CH-1700 Fribourg, Switzerland
§ Department of Physics and Astronomy, University of Nebraska, Lincoln, NE 68588-0111, USA
£ Institute of Physical and Theoretical Chemistry, Technical University of Munich, D-85747 Garching, Germany

Abstract. Vibrational excitation of HF by low-energy electrons has been investigated experimentally and theoretically. A new nonlocal resonance model has been constructed based on *ab initio* calculations of the coupling between a discrete state and continuum states. Vibrational excitation and resonant elastic cross sections have been calculated for a set of initial vibrational states of the molecular target. New high-resolution measurements of vibrational excitation cross sections for the transitions $v = 0 \to 1, ..., v = 0 \to 4$ have been carried out. The calculated cross sections are in good agreement with the experimental data, indicating that the mechanisms responsible for the rich threshold structures in the collision cross sections for hydrogen fluoride are well understood.

PACS numbers: 34.80.Gs

1. Introduction

The discovery of pronounced threshold peaks in the vibrational excitation (VE) cross sections of HF, HCl and HBr by Rohr and Linder about 25 years ago [1]-[3] has initiated extensive experimental and theoretical research on low-energy collisions of electrons with hydrogen halides. The experimental studies unveiled a multitude of interesting phenomena. Related to the threshold peaks are cusps at vibrational thresholds in the elastic [4] and inelastic [1]-[3] channels and step-like structures at VE thresholds in the cross section for dissociative attachment (DA) [5, 6, 7], which have been discovered at about the same time as the threshold peaks. The structures in the DA cross section have been interpreted in terms of vibrational channel openings by Fiquet-Fayard [8]. Narrow interference structures in the $v = 0 \rightarrow 1, 2, 3$ cross sections of HF have been observed by Knoth *et al* [9] and assigned to vibrational Feshbach resonances. A series of detailed studies of rovibrational excitation cross sections of HF and HCl has subsequently been performed by Ehrhardt and coworkers (Ref. [10] and references therein).

More recently, not only more accurate determinations of the shape and intensity of the threshold peaks and cusp structures in the VE functions of hydrogen halides have become possible, but also additional unexpected phenomena have been discovered. Cvejanović and Jureta [11] and Cvejanović [12] reported narrow oscillatory structures in the $v = 0 \rightarrow 1$ and $v = 0 \rightarrow 2$ VE cross sections of HCl. The existence of these oscillations has been confirmed by Schafer and Allan [13]. Very recently, these narrow oscillatory structures have been revealed with much better resolution in both HCl and HBr by applying rotational cooling of the target gas [14, 15]. New results have been obtained for HF by extension of the measurements up to the $v = 4$ channel, revealing the existence of oscillatory structures also in this system [16].

The experimental research on low-energy electron scattering from hydrogen halides has been accompanied by intense theoretical efforts over many years. A variety of theoretical concepts and methods have been developed to explain the experimental findings, among them rovibrational close-coupling expansions [17, 18, 19], extensions of the R-matrix method to account for nuclear dynamics [20, 21, 22], effective-range models [23] and the so-called nonlocal resonance model based on the Feshbach projection-operator approach [24]. A complete survey of the theoretical developments can be found in reviews by Morrison [25], Fabrikant [26], Domcke [27] and Horáček [28]. The most recent developments in the joint theoretical and experimental investigation of VE and dissociative attachment in low-energy electron collisions with HCl and HBr are reviewed in [29].

In the present article we report on our experimental and theoretical work on vibrational excitation of HF. The absolute VE cross sections have been measured with an extended precision for the transitions $v = 0 \rightarrow 1, ..., v = 0 \rightarrow 4$. A new nonlocal resonance model has been constructed, based on a recent calculation of the HF^- potential surface by Piecuch [30] and the *ab initio* calculation of the coupling between the discrete Σ state of HF^- and the continuum [31]. Detailed studies of the dissociative attachment cross section for HF were presented in Refs. [31, 32].

2. Experimental methods

The measurements were performed using a spectrometer with hemispherical analysers described in more detail in in Refs. [14, 15]. The response function of the spectrometer was determined on the elastic and the 2^3S excitation cross sections of helium. The correction for the response function is accurate within about ±25% over the energy range presented here, but less accurate within the first 200 meV above threshold. The resolution was about 20 meV in the energy-loss mode, about 14 meV in the incident energy. The cross sections were measured at the maxima of the energy-loss bands, that is, they emphasise $\Delta J = 0$ the transitions. Preliminary values of the relative cross sections for different final vibrational states were determined from an energy-loss spectrum recorded at a residual energy of 0.15 eV. The experiment measures differential cross sections at 90°, but comparison of shapes with calculated integral cross sections is justified by the expectation of a dominant s-wave and largely isotropic scattering in HF at low energies.

3. Nonlocal resonance model

3.1. General theory

The nonlocal resonance model is based on the assumption that a temporary molecular negative-ion state (resonance) is formed and that this resonance accounts for the coupling of the electronic scattering dynamics with the nuclear motion [33]. The resonance is represented by a square-integrable discrete state $|\varphi_d\rangle$ which interacts with a continuum of scattering states $|\varphi_\epsilon\rangle$ via coupling matrix elements $V_{d\epsilon}$. $|\varphi_d\rangle$ and $|\varphi_\epsilon\rangle$ are assumed to be diabatic states, that is, their wave functions vary smoothly with the internuclear distance R and the coupling of these states due to the nuclear kinetic energy operator $T_N = -\frac{1}{2\mu}\Delta_R$ can be neglected. The second essential ingredient of the nonlocal resonance model for hydrogen halides is the explicit consideration of threshold effects induced by the long-range dipole potential. The dipole-induced nonanalyticities of the S matrix and related quantities at threshold enter through the threshold expansion of the energy-dependent width function

$$\Gamma(\epsilon) = 2\pi |V_{d\epsilon}|^2 \tag{1}$$

and the associated level shift $\Delta(\epsilon)$ [33].

The basic equation of the nonlocal resonance theory is the wave equation describing nuclear motion in the short-lived anion state [27, 34]

$$\begin{aligned} &[T_N + V_d(R) - E]\Psi_d(R) + \\ &\int d\epsilon \int dR' V_{d\epsilon}(R) G_0(R, R'; E-\epsilon) V^*_{d\epsilon}(R')\Psi_d(R') = -V_{d\epsilon_i}(R)\chi_{v_i}(R) \end{aligned} \tag{2}$$

with

$$G_0(R,R';E) = \langle R \mid (E - T_N - V_0 + i\varepsilon)^{-1} \mid R'\rangle. \quad (3)$$

Here $V_0(R)$ and $V_d(R)$ are the potential-energy functions of the target state and the discrete state, respectively. $\chi_{v_i}(R)$ is the wave function of the initial vibrational state of the target molecule, ϵ_i is the energy of the incoming electron, and E is the total energy of the collision complex. G_0 is the Green's function for nuclear motion in the target state, T_N being the radial nuclear kinetic energy operator.

The second term on the left hand side of Eq.(2) plays the role of a complex, energy-dependent and nonlocal effective potential for the radial nuclear motion. It accounts for the decay of the electronic resonance state through the coupling with the electronic scattering continuum.

From the solution of Eq.(2), the integral cross section for electron scattering from initial vibrational state v_i to final state v_f is obtained as [27]

$$\sigma_{v_f v_i}(E) = \frac{4\pi^3}{k_i^2}|\langle\chi_{v_f}|V^*_{d\epsilon_f}|\Psi_d\rangle|^2. \quad (4)$$

This expression includes only the resonant part of the scattering amplitude, which is dominant for inelastic processes.

3.2. Nonlocal resonance model for HF

The nonlocal resonance model proved to be extremely successful for the treatment of low-energy resonant electron collisions with HCl and HBr molecules [15, 35]. An essential ingredient of this success is the use of the correct energy dependence of the resonance width at threshold which is given by a modification of the Wigner threshold law [36]. According to this modification [37], at energies near threshold

$$\Gamma(\epsilon) \sim \epsilon^\alpha \quad (5)$$

where α is so called threshold exponent. In the case of polar molecules this exponent is determined by the dipole moment of the target molecule. Since the dipole moment of the molecule changes as the molecule vibrates, the threshold exponent is a function of the internuclear distance R. For a precise description of the VE cross sections at thresholds it is necessary to take this dependence into account [38]. At the equilibrium distance, the threshold exponent attains the values 0.48 for HI, 0.42 for HBr and 0.36 for HCl. The threshold exponent is real for these molecules and hence $\Gamma(\epsilon)$ is a smooth, but rapidly rising function of the energy close to threshold. HF however, in contrast to HCl, HBr and HI molecules, possesses a supercritical dipole moment and the threshold exponent becomes complex. For supercritical dipole moments the width takes the form [31, 37]

$$\Gamma(\epsilon) = \frac{const.}{1 + e^{2\pi\mu} + 2e^{\pi\mu}cos(\mu\ln\epsilon + \gamma)} \quad (6)$$

where μ depends only on the dipole moment, and γ both on dipole moment and the short-range interaction.

The nonlocal resonance model is characterised by the three functions $V_0(R), V_d(R)$ and $V_{d\epsilon}(R)$. The target potential-energy function $V_0(R)$ can directly be obtained by *ab initio* calculations or by fitting spectroscopic data. The functions $V_d(R)$ and $V_{d\epsilon}(R)$ representing the HF$^-$ resonance (at short internuclear distance) and the HF$^-$ bound state (at intermediate and large internuclear distances) have been obtained by a joint fitting of the *ab initio* calculation of the coupling of the discrete state with the orthogonalised continuum [31] and accurate *ab initio* calculations [30] of the HF$^-$ potential-energy function at intermediate internuclear distances. All parameters of the model are thus determined by *ab initio* calculations. The basic quantity of the nonlocal resonance model, the nonlocal potential $F(E - T_N - V_0, R, R')$ (see the second term in Eq. (2)), is defined in terms of the coupling $V_{d\epsilon}(R)$ as

$$
\begin{aligned}
F(\epsilon, R, R') &= \int d\epsilon' V_{d\epsilon'}(R)(\epsilon - \epsilon' + i\varepsilon)^{-1} V^*_{d\epsilon'}(R') \\
&= \Delta(\epsilon, R, R') - \frac{i}{2}\Gamma(\epsilon, R, R'), \qquad (7)
\end{aligned}
$$

where

$$\Gamma(\epsilon, R, R') = 2\pi V_{d\epsilon}(R) V^*_{d\epsilon}(R'), \qquad (8)$$

$$\Delta(\epsilon, R, R') = P \int d\epsilon' \Gamma(\epsilon', R, R')(\epsilon - \epsilon')^{-1}. \qquad (9)$$

The work of Gallup et al. [31] provides restricted widths and level shifts $\Gamma(\epsilon, R) \equiv \Gamma(\epsilon, R, R' = R)$ and $\Delta(\epsilon, R) \equiv \Delta(\epsilon, R, R' = R)$ for a set of values of the internuclear distance R, 1.5 a.u.$< R < -2.5$ a.u., and for a set of energies in the range (-5.0,5.0) eV. The restriction $R = R'$ is sufficient for the semiclassical approach employed in Ref. [31]. In order to evaluate the effective potential $F(\epsilon, R, R')$ needed for fully quantum treatment of the problem, we parameterised their data assuming the following separable form of $\Gamma(\epsilon, R)$and $\Delta(\epsilon, R)$:

$$\Gamma(\epsilon, R) = \gamma(\epsilon)|g(R)|^2, \qquad (10)$$

$$\Delta(\epsilon, R) = \delta(\epsilon)|g(R)|^2. \qquad (11)$$

Using these quantities we define "full" nonlocal operators as

$$\Gamma(\epsilon, R, R') = g(R)\gamma(\epsilon)g(R')^*, \qquad (12)$$

$$\Delta(\epsilon, R, R') = g(R)\delta(\epsilon)g(R')^*. \qquad (13)$$

It is obvious that from $\Gamma(\epsilon, R)$ we cannot determine the complex phase of $g(R)$. Nevertheless, for diabatic states $|\varphi_d\rangle$, $|\varphi_\epsilon\rangle$ this quantity is a slowly varying function of R and can be neglected in $\Gamma(\epsilon, R, R')$ and $\Delta(\epsilon, R, R')$. We therefore assume that $g(R)$ is real. The representation of the integral kernels $\Gamma(E, R, R')$ and $\Delta(E, R, R')$ in this separable form is of course approximate, but is known to be a good first approximation for many molecules. In addition, this separable form greatly simplifies the numerical calculation [39]. We fitted the functions $\gamma(\epsilon)$, $\delta(\epsilon)$ for $\epsilon > 0$ and $\delta(\epsilon)$ for $\epsilon < 0$ separately in the form of Padé [1/2] approximation ($\gamma = 0$ for $\epsilon < 0$)

$$P[1/2](\epsilon) = \frac{a\epsilon + b}{\epsilon + c + d\epsilon^2}. \tag{14}$$

The analytic behaviour of the functions γ and δ for HF, a molecule with a strong dipole moment, has been discussed in [31]. Here we only recall that the functions γ and δ are rapidly oscillating functions of energy at $\epsilon \approx 0$. These oscillations are, however, limited to a very narrow region close to $\epsilon = 0$ (comparable to the rotational spacing). For the description of the present experiment it is sufficient to assume that the functions γ and δ are smooth near the origin and have a step behaviour at $\epsilon = 0$. The function $g(R)$ is taken to be of the Gaussian form

$$g(R) = A_1 \exp(-\alpha_1 (R - R_1)^2). \tag{15}$$

The constants a, b, c, d and A_1, α_1, R_1 were obtained by least-squares fit to the values of $\Gamma(\epsilon, R)$ and $\Delta(\epsilon, R)$ from [31] for eight internuclear distances R in the range 1.5-2.5 a.u. and for energies $\epsilon = -5, -4.9, -4.8..., 5$ eV. The values of the constants are given in Table 1. The fit reproduces the data for $\Gamma(\epsilon, R)$ within $\pm 5\%$ and the data for $\Delta(\epsilon, R)$ within $\pm 10\%$, see figure 1.

For the calculation of VE cross sections it is necessary to define the function $g(R)$ also at distances larger than 2.5 a.u. Like in our previous calculations for HCl [35], a reliable representation of the function $g(R)$ can be obtained if the discrete-state potential $V_d(R)$ is constructed consistently with the *ab initio* HF^- adiabatic potential. It has been shown recently that the long-range behaviour of the discrete-state potential $V_d(R)$ essentially determines the behaviour of the VE cross section below DA threshold [14]. To find a good representation of $V_d(R)$ at larger internuclear distances, we used the *ab initio* data for the adiabatic potential energy of the HF^- [30]. The fitting procedure is described in [35]. The resulting potential joins the polarisation potential $-2.25R^{-4}$ at large R. The ab initio data for the adiabatic potential energy extend down to $R = 2$ a.u. and hence overlap with the data of [31]. The data in the overlap region are not fully mutually consistent because of the Hartree-Fock approximation used by Gallup *et al* [31]. The difference is, however, small and this uncertainty does not affect much the resulting cross sections.

We assume the discrete-state potential to be of the form

$$V_d(R) = -2.25 \frac{R - v_1}{R^5 + v_2 R^4 + v_3 R^2} \quad \text{for } R > R_0, \tag{16}$$

$$= A_d e^{-2\alpha_d (R - R_d)} + p + qR \quad \text{for } R < R_0. \tag{17}$$

The constants v_1, v_2 and v_3 have been fitted to reproduce the *ab initio* HF^- potential for $R > 2.3$; their values are given in Table 1. The constants p and q are chosen in such a way that both forms of $V_d(R)$ merge smoothly at $R = R_0$. The parameter R_0 can be varied to test the sensitivity of the results. The choice $R_0 = 3.4$ a.u. represents the best compromise which describes reasonably well all the available *ab initio* data.

Table 1. Model parameters (in atomic units). The first part gives values of Padé approximation coefficients (see equation (14)) for the energy dependence of the width $\Gamma = \gamma(\epsilon)g(R)^2$ and level shift $\Delta = \delta(\epsilon)g(R)^2$ functions. The Gaussian fit (15) for $g(R)$ and the discrete-state potential (16)-(17) are shown in the second and third parts respectively.

γ/δ	$\gamma(\epsilon > 0)$	$\delta(\epsilon > 0)$	$\delta(\epsilon < 0)$
a	0.227	0.734	-0.0677
b	0.00235	-0.177	0.00123
c	0.0590	1.528	-0.0104
d	-0.728	-19.4	-3.93
$g(R)$	$A_1 = 1.31$	$\alpha_1 = -0.1233$	$R_1 = 0.25$
$V_d(R)$	$v_1 = 2.99973$	$v_2 = -4.45722$	$v_3 = 32.6758$
	$A_d = 0.03307$	$\alpha_d = 1.8638$	$R_d = R_0$

The exponential term in the expression for $V_d(R)$ for $R < R_0$ comes from the original potential of [31].

The potential-energy functions of the target molecule and the negative ion, which are very useful for a qualitative interpretation of the observed structures in the cross sections, are shown in figure 2, together with the *ab initio* data for the bound part of the anion potential-energy functions. Unlike HCl^- and HBr^-, the HF^- potential function does not have a proper 'outer well', separated by a potential barrier. Very narrow 'outer well resonances' reported for HCl and HBr [14, 15], that is quasi-stationary vibrational levels, the wave function of which is located primarily in the outer well of the potential-energy function, are consequently missing in the HF cross sections. Instead of the outer well, there is a section of the HF^- potential which rises only very gradually and extends to large R. It supports a number of quasi-bound vibrational levels which converge towards the dissociative attachment threshold.

The causes of the absence of the outer well in the HF^- potential curve can be understood with the following qualitative arguments. The $\mathrm{H}X^-$ adiabatic curve is dominated by the H–X^- forces at large R and the e^-–HX interaction at smaller R. The range of R where the transition occurs depends on two factors: the dipole moment of HX and the size of the ion X^-. To be specific, let us compare HF^- and HCl^-. At very large distances, the polarisation interaction dominates in both cases. At smaller distances, H–Cl^- valence repulsion takes over, and this creates an outer well. However, at this distance the valence shells of H and F^- do not overlap yet, and if we go to somewhat smaller distances, the dipole interaction takes over, and the HF^- curve remains attractive.

4. Results and Discussion

The measured vibrational excitation cross sections for the transitions $v = 0 \to 1, ..., 4$ are plotted in figure 3. The data for up to $v = 3$ agree well with those of Ehrhardt and coworkers [9]. All final vibrational states were recorded with the same instrumental settings and consequently the same resolution in the present experiment. This represents an improvement over the measurements of Ehrhardt and coworkers where the $v = 0 \to 3$ channel was measured with higher sensitivity, reduced resolution conditions, and the onset appeared less steep, without a proper threshold peak. The onsets of all curves are now seen to be equally steep, with signals peaking about 45 meV above the thresholds. This is compatible with truly vertical onsets, given the resolution of the experiment and the limited capacity of the analyser to detect electrons with less than about 50 meV energy. The present data also agree well with those of Sergenton *et al* [16], but represent an improvement in resolution. While the data of Sergenton *et al* did not show a proper threshold peak in the $v = 0 \to 4$ channel, the present results show that the signal onset is vertical and the threshold peak is found even there, but its height is 'suppressed' by the close lying deep dip in the cross section. The higher resolution permitted a better calibration of the energy scale of the $v = 4$ cross section. This reveals an 'amplitude inversion' between the $v = 3$ and $v = 4$ signals: peaks are observed in the $v = 3$ signal at exactly the same energies as dips in the $v = 4$ signal and *vice versa*. The small shift of the structures reported by Sergenton *et al* [16] was due to slight imperfection of the energy scale calibration for the $v = 4$ channel. This inversion relation is also observed for the 1.73 eV structure originally described by Ehrhardt and coworkers [9] which appears as a deep dip in the $v = 3$ channel and as a peak in the $v = 2$ channel.

The theoretical VE cross sections are shown in figure 4. The overall agreement of the theory with the experiment is very good. It is emphasised by the detailed comparison of the $v = 0 \to 3$ cross sections in figure 5. Note that theory and experiment agree extremely well on the width and the depth of the dip around 1.7 eV. Agreement is also very good for the shape of the threshold peak.

The theoretical spectra show two types of structures. The first are very sharp drops of the signal observed in each channel exactly at the vibrational threshold of the next higher channel, for example the $v = 2$ threshold in the $v = 0 \to 1$ cross section, or at the $v = 4$ threshold in the $v = 0 \to 3$ cross section, and finally at the $v = 5$ threshold in the $v = 0 \to 4$ cross section. These structures are too narrow to be verified explicitly by the present experiment, except in the case of the $v = 2$ threshold in the $v = 0 \to 1$ cross section. The second type of structure are dips and peaks which are narrow at lower energies (for example, the dip at 1.40 eV in the $v = 0 \to 2$ channel), but become broader at higher energies (for example the dip at 1.732 eV in the $v = 0 \to 3$ channel), until their widths approach their separations and they become boomerang oscillations at the $v = 0 \to 3$ and $v = 0 \to 4$ cross sections above 2.0 eV. These structures, assigned to vibrational Feshbach resonances (VFRs), are fully confirmed by the experiment. Whereas the lower-lying VFR have a clearly defined parent vibrational state, the concept of parent vibrational level becomes less meaningful at higher energies where the VFR overlap. The low-lying VFRs are very close to their parent vibrational level. The dip at 1.399 eV (in the $v = 0 \to 2$ cross section) is only 11 meV below its parent $v = 3$ level (which is at 1.410 eV). The dip 1.732 eV (in the $v = 0 \to 3$ cross section) is already 108 meV below its $v = 4$ parent level. There is a slight difference between theory and experiment in the position of the structures. The lower-lying VFR are measured at slightly higher energies than calculated. The calculated position of the $v = 3$ VFR is 35 meV whereas experimentally it was found at 11 meV – the difference is barely outside the error limit of the experimental energy scale calibration, however. The difference is significant for the next VFR, whose calculated position is 160 meV, whereas experimentally it was found at 108meV below its parent $v = 4$ vibration (figure 5). In contrast, the higher-lying oscillatory structures were found at slightly higher energies than those measured (figure 5). These differences can be considered as minor, however, in view of the fact that the positions are a sensitive function of the details of the shape of the HF^- potential curves which has no adjustable parameters in the present calculation.

The present results elaborate in detail and fully confirm the qualitative explanation of the structures in terms of vibrational Feshbach resonances put forward by Ehrhardt and coworkers [9]. Note that a third kind of structure, the 'outer well resonances' found in HCl and HBr, is absent in HF, because the potential has no outer well.

Another quantity which can be compared between theory and experiment are the relative magnitudes of the cross sections. Theory and experiment agree qualitatively on the fact that the cross sections drop very rapidly with increasing vibrational quantum. The agreement is not quantitative, however: the experimental cross sections drop faster with rising final v.

In the majority of theoretical approaches employed for the description of the the near-threshold vibrational excitation of hydrogen halides it is necessary to fit some parameters of the models to certain experimental data to obtain even a qualitative agreement with the measurement. We wish to emphasise that in the present calculation no parameters were fitted to experimental data and only *ab initio* data were used. As mentioned in Section 3.2, the present model approximates the threshold behaviour of the width function $\Gamma(E)$ by a smooth function of the energy, while the exact width exhibits an infinite number of oscillations in the approximation of the fixed molecular orientation. It has been shown for HCl and HBr that to obtain the correct shape of the cross sections very close to thresholds, it is necessary to take into account the precise form of the width. Since in the present case the threshold behaviour is approximate, one cannot expect a perfect agreement for energies very close to the threshold, but a good agreement at somewhat higher energies. This is true in the present case. The measured data agree better with the experiment at higher energies. The agreement also improves for higher transitions $v = 0 \to 2, 3$ and 4.

The rotational temperature of the molecular target was assumed to be $T = 0$ K in the calculation shown in figures 3 and 5. In a real experiment, however, the temperature was about 300 K. To check the sensitivity of the results to changes of the rotational target temperature we calculated the $0 \to 1$ VE cross section for various rotational states. For each angular momentum J we repeated the calculation of the cross section with $V_0(R)$ and $V_d(R)$ augmented by $J(J+1)/2\mu R^2$. The finite temperature of the target gas is taken into account by averaging over the Maxwell-Boltzmann distribution of rotational states of the target molecule for $T = 300$ and $T = 1000$ K. The effect of increasing temperature on the VE cross sections is found to be small. Similarly, we verified that taking into account the finite energy resolution $\Delta E = 50$ meV of the incident electron beam leads to small changes of the VE cross section. Much more important is the uncertainty in the input parameters of the model. As we mentioned before, the two *ab initio* data sets for small and large R used to define the model are not fully consistent in the overlap region. We use the parameter R_0 in the model to control this ambiguity. Sensitivity of the results to changes in this parameter are shown in figure 6. The same figure also shows the VE cross sections calculated for the original model [31] with the separable representation of $\Gamma(\epsilon, R)$ and $\Delta(\epsilon, R)$, but without the modification of $V_d(R)$ according to the data for fixed-R HF^- energies in the region where the anion state is electronically bound.

In figure 7 we plot the resonance contribution to the elastic scattering of electrons on HF for molecules in the ground state and in vibrationally excited target states. Cusps at openings of new vibrational channels are clearly discernible. The overall shape and the cusp at the $v = 1$ threshold are well confirmed for the target in the ground state by the experimental spectrum in figure 8. Remarkable is the deep minimum in the $2 \to 2$ channel below the opening of the $2 \to 3$ channel. No experiments are available for this channel so far.

In figure 9, the three VE cross sections $0 \to 1$, $1 \to 2$ and $2 \to 3$ are shown. Although the excitation energies of all these processes are almost identical, the magnitude of the VE cross section increases rapidly with increasing initial vibrational quantum.

5. Conclusions

HF represents, after HCl [14] and HBr [15], another case where threshold peaks and a multitude of near-threshold structures can be explained quantitatively by a single (albeit energy-dependent and nonlocal) anion potential-energy function. The significance of the present study resides in the fact that it tests the model with substantially different parameters – HF has, unlike HCl and HBr, a supercritical dipole moment and the threshold exponent is complex. Furthermore, the HF^- potential well is deeper than in the HCl and HBr cases, and demonstrates thus in a particularly nice way the gradual transition from very narrow vibrational Feshbach resonances at low energies to boomerang oscillatory structures close to the DA limit. An important difference is that the HF^- potential does not have an outer well, in contrast to HCl^- and HBr^-. The high degree of agreement between experiment and theory in the case of HF further substantiates the nonlocal resonance model and confirms the high quality of the underlying *ab initio* calculations.

HF represents a useful prototype for the qualitative understanding of near-threshold structures in larger molecules where they cannot be calculated at present. It demonstrates clearly and quantitatively how narrow VFR occur even when there is no bound adiabatic curve of the anion for the entire range of internuclear separations and how sharp structures at low energies gradually turn to boomerang oscillations at higher energies. Structures with the same qualitative behaviour were recently discovered in CO_2 [40] and N_2O [41].

6. Acknowledgement

This research was sponsored by GAČR 203/00/1025, GAČR 203/00/D111 and by project No. 2000-067877.02 of the Swiss National Science Foundation, and by U.S. National Science Foundation, grant No. PHY-0098459.

References

[1] Rohr K and Linder F 1975 *J. Phys. B: At. Mol. Phys.* **8** L200
[2] Rohr K and Linder F 1976 *J. Phys. B: At. Mol. Phys.* **9** 2521
[3] Rohr K 1978 *J. Phys. B: At. Mol. Phys.* **11** 1849
[4] Burrow P D 1974 *J. Phys. B: At. Mol. Phys.* **7** L385
[5] Ziesel J P, Nenner I and Schulz G J 1975 *J. Chem. Phys.* **63** 1943
[6] Abouaf R and Teillet-Billy D 1977 *J. Phys. B: At. Mol. Phys.* **10** 2261
[7] Abouaf R and Teillet-Billy D 1980 *Chem. Phys. Lett.* **73** 106
[8] Fiquet-Fayard F 1974 *J. Phys. B: At. Mol. Phys.* **7** 810
[9] Knoth G, Gote M, Rädle M, Jung K and Ehrhardt H 1989 *Phys. Rev. Lett.* **62** 1735
[10] Ehrhardt H 1989, in: A. Herzenberg (ed), Aspects of Electron-Molecule Scattering and Photoionization, American Institute of Physics, New York, AIP Conf. Proc. **204**, 145
[11] Cvejanović S and Jureta J 1989, Abstracts of the 3rd Eur. Conf. on Atomic and Molec. Phys. (Bordeaux) p. 638
[12] Cvejanović S 1993, in: T Andersen, B Fastrup, F Folkmann, H Knudsen and N Anderson (Eds.), The Physics of Electronic and Atomic Collisions (18th ICPEAC, Aarhus), American Institute of Physics, New York, AIP Conf. Proc. **295**, 390
[13] Schafer O and Allan M 1991 *J. Phys. B: At. Mol. Opt. Phys.* **24** 3069
[14] Allan M, Čížek M, Horáček J and Domcke W 2000 *J. Phys. B: At. Mol. Opt. Phys.* **33** L209
[15] Čížek M, Horáček J, Sergenton A-Ch, Popović D B, Allan M, Domcke W, Leininger T and Gadea F X 2001 *Phys. Rev.* A **63** 062710
[16] Sergenton A-Ch, Jungo L and Allan M 2000 *Phys. Rev.* A **61** 062702
[17] Thümmel H T, Nesbet R K and Peyerimhoff S D 1993 *J. Phys. B: At. Mol. Opt. Phys.* **26** 1233
[18] Rudge M R H 1980 *J. Phys. B: At. Mol. Phys.* **13** 1269
[19] Rescigno T N, Orel A E, Hazi A U and McKoy B V 1982 *Phys. Rev.* A **26** 690
[20] Morgan L A, Burke P G and Gillan C Z 1990 *J. Phys. B: At. Mol. Opt. Phys.* **23** 99
[21] Fabrikant I I, Kalin S A and Kazansky A K 1992 *J. Phys. B: At. Mol. Opt. Phys.* **25** 2885
[22] Morgan L A and Burke P G 1988 *J. Phys. B: At. Mol. Opt. Phys.* **21** 2091
[23] Teillet-Billy D and Gauyacq J P 1984 *J. Phys. B: At. Mol. Phys.* **17** 4041
[24] Domcke W and Mündel C 1985 *J. Phys. B: At. Mol. Phys.* **18** 4491
[25] Morrison M A 1988 *Adv. At. Mol. Phys.* **24** 51

[26] Fabrikant I I 1999 in: The Physics of Electronic and Atomic Collisions (XXI ICPEAC, Sendai), eds. Y. Itikawa *et al* American Institute of Physics, New York, p 270
[27] Domcke W 1991 *Phys. Rep.* **208** 97
[28] Horáček J 1999 in: The Physics of Electronic and Atomic Collisions (XXI ICPEAC, Sendai), Eds. Y. Itikawa *et al*, American Institute of Physics, New York, p 329
[29] Čížek M, Horáček J, Allan M and Domcke W 2002 *Czech. J. Phys.* **52** 1057
[30] Piecuch P 1997 *J. Mol. Struct.* **436-437** 503
[31] Gallup G A, Xu Y and Fabrikant I I 1998 *Phys. Rev.* A **57** 2596
[32] Xu Y, Gallup G A, and Fabrikant, I I 2000 *Phys. Rev.* A **61** 052705
[33] Domcke W and Cederbaum L S 1981 *J. Phys. B: At. Mol. Phys.* **14** 149
[34] Bardsley J N 1968 *J. Phys. B: At. Mol. Phys.* **1** 349
[35] Čížek M, Horáček J and Domcke W 1999 *Phys. Rev.* A **60** 2873
[36] Wigner E P 1948 *Phys. Rev.* **73** 1002
[37] Fabrikant I I 1977 *Sov. Phys. JETP* **46** 693
[38] Horáček J, Čížek M and Domcke W 1998 *Theor. Chem. Acc.* **100** 31
[39] Pichl L, Nakamura H and Horáček J 2000 *Comp. Phys. Comm.* **124** 1
[40] Allan M 2002 *J. Phys. B: At. Mol. Opt. Phys.* **35** L387-L395
[41] Allan M 2003 in preparation

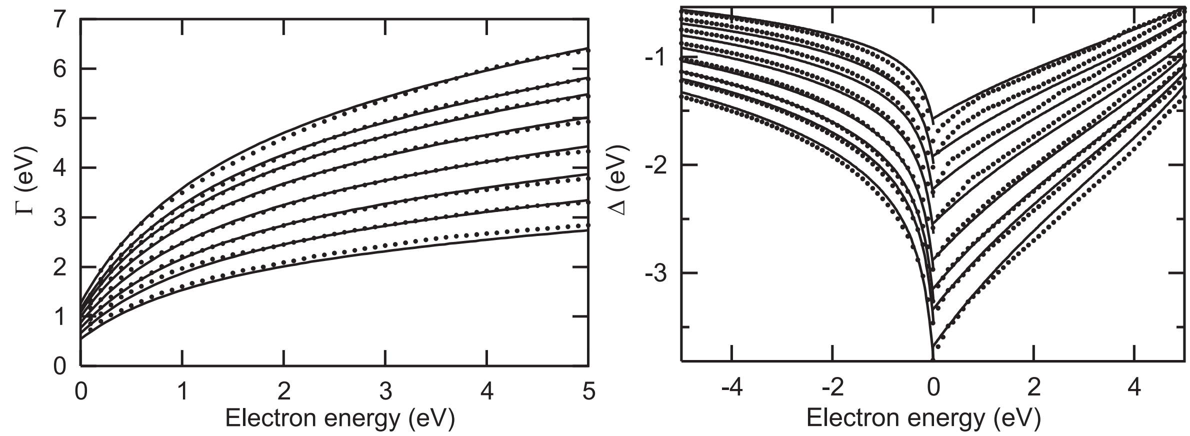

Figure 1. Separable fit (lines) of *ab initio* data (dots) for $\Gamma(\epsilon, R)$ and $\Delta(\epsilon, R)$ for $R = 1.5, 1.65, 1.73, 1.85, 2.0, 2.15, 2.3$ and 2.49 (from top to bottom for Γ and from bottom to top for Δ).

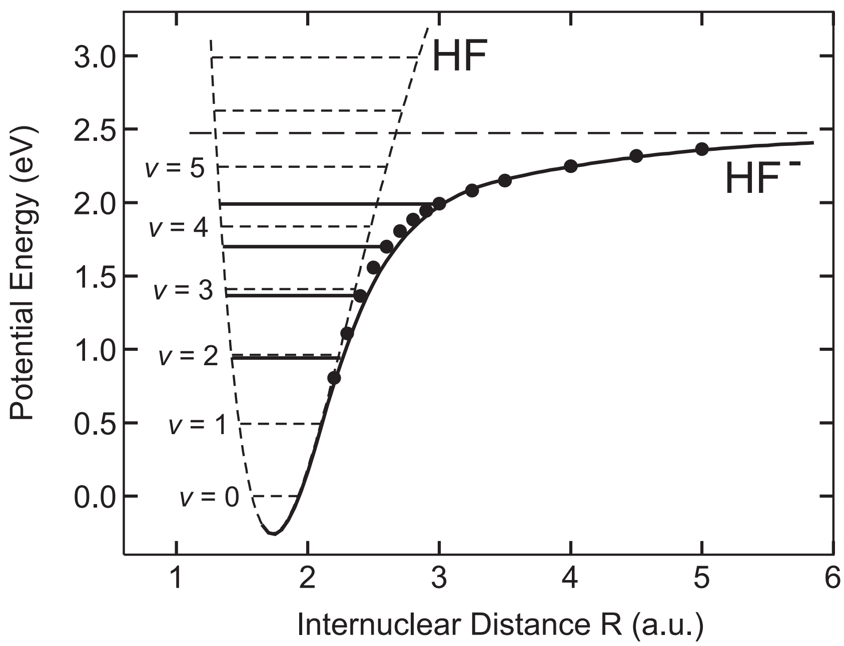

Figure 2. Adiabatic potential curves for HF (dashed) and HF^- (solid line). *Ab initio* data [30] are shown with circles. Positions of vibrational Feshbach resonances are indicated schematically by solid horizontal lines.

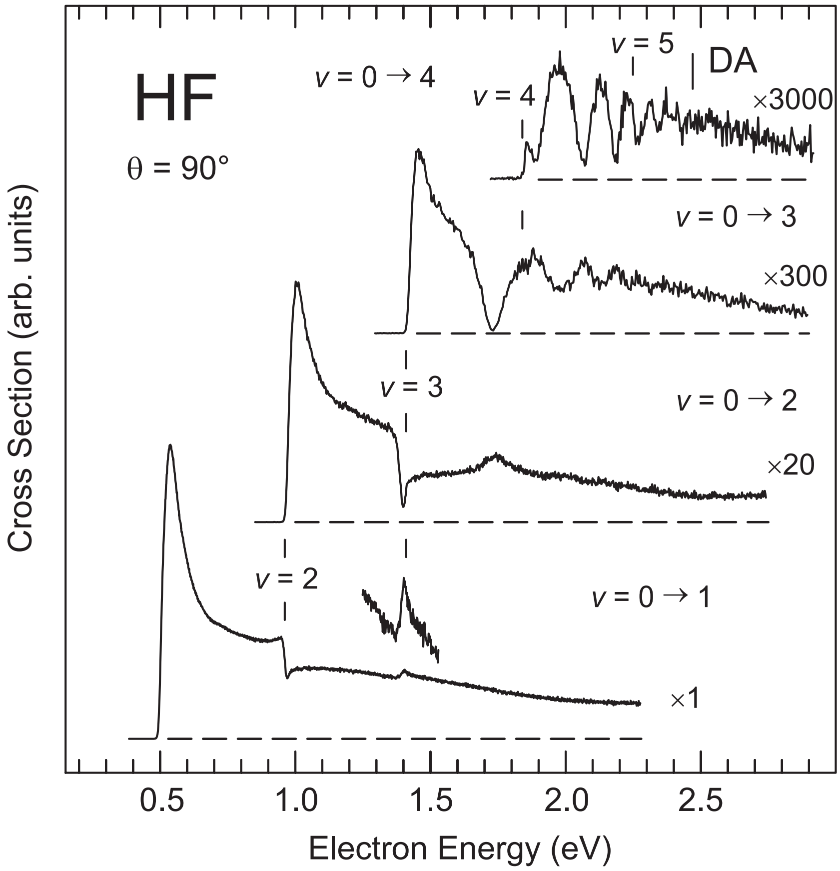

Figure 3. Measured VE cross sections. Vibrational and DA thresholds are marked.

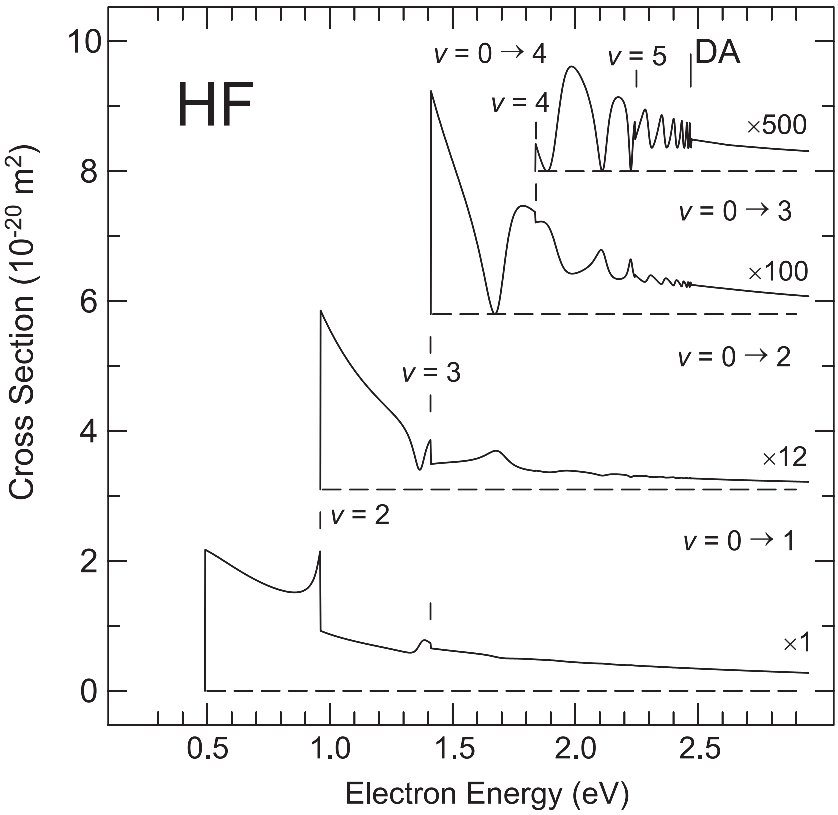

Figure 4. Calculated VE cross sections. Vibrational and DA thresholds are marked.

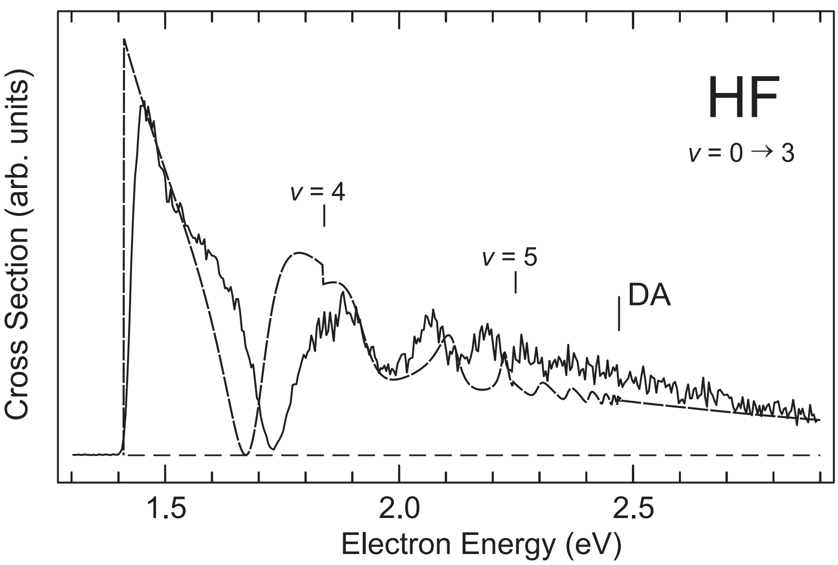

Figure 5. Calculated (dashed) and measured VE $v = 0 \rightarrow 3$ cross sections.

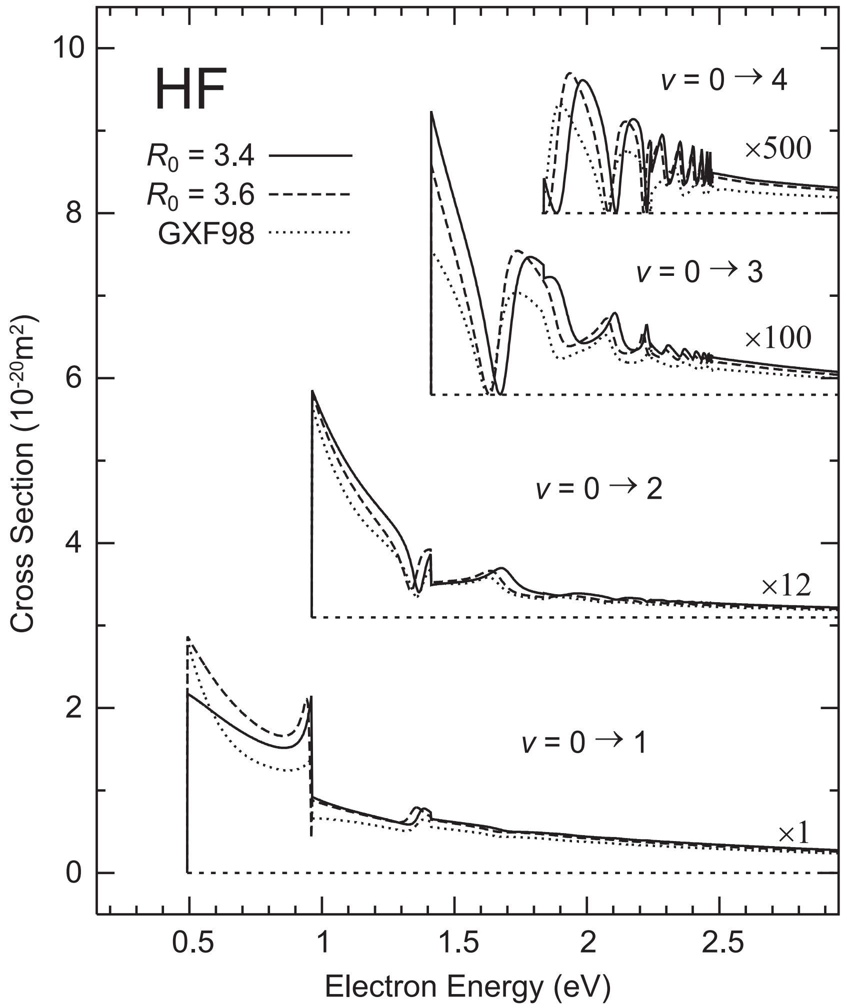

Figure 6. Sensitivity of the VE cross sections to the point R_0 and cross sections for original model [31] (labelled GXF98).

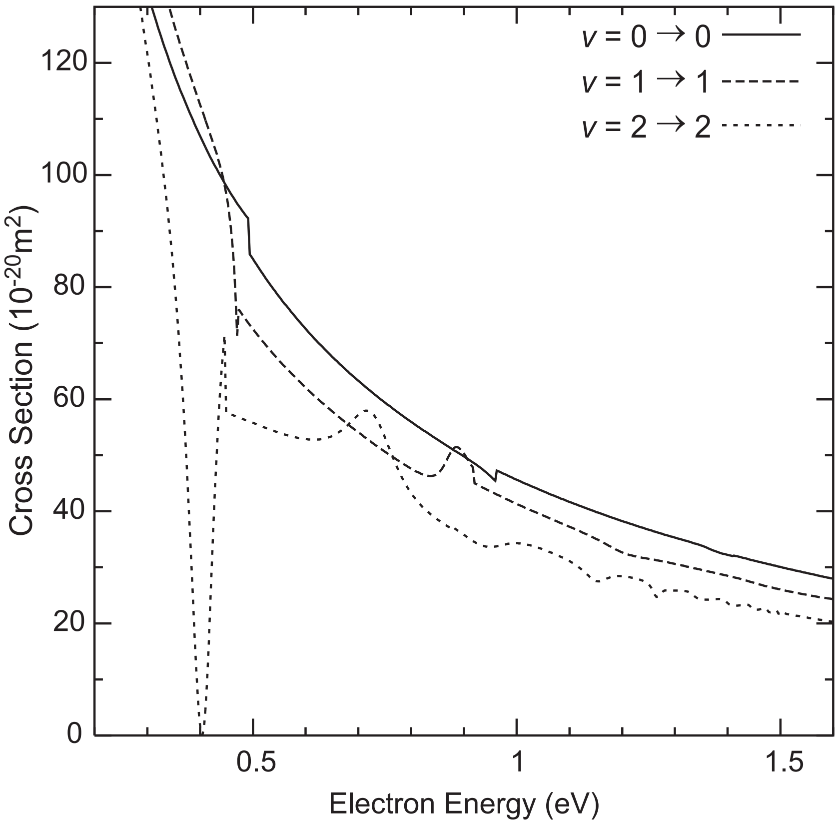

Figure 7. Resonance contribution to the elastic scattering for vibrationally excited molecules.

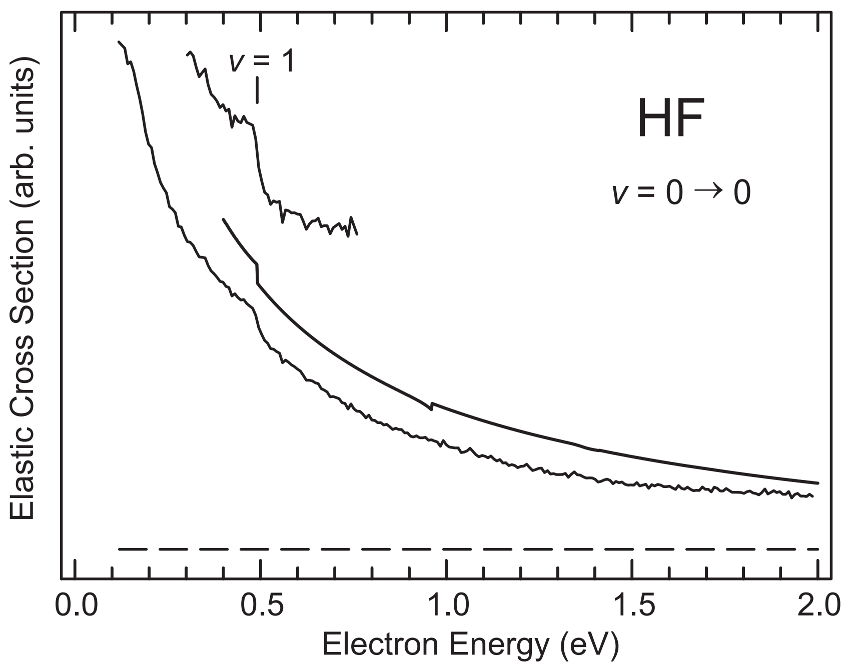

Figure 8. Measured elastic cross section and the calculated resonance contribution to the elastic scattering (smooth curve), for HF in the ground vibrational state. A section of the experimental spectrum is shown tilted and vertically expanded to emphasise the structure at the $v = 1$ threshold.

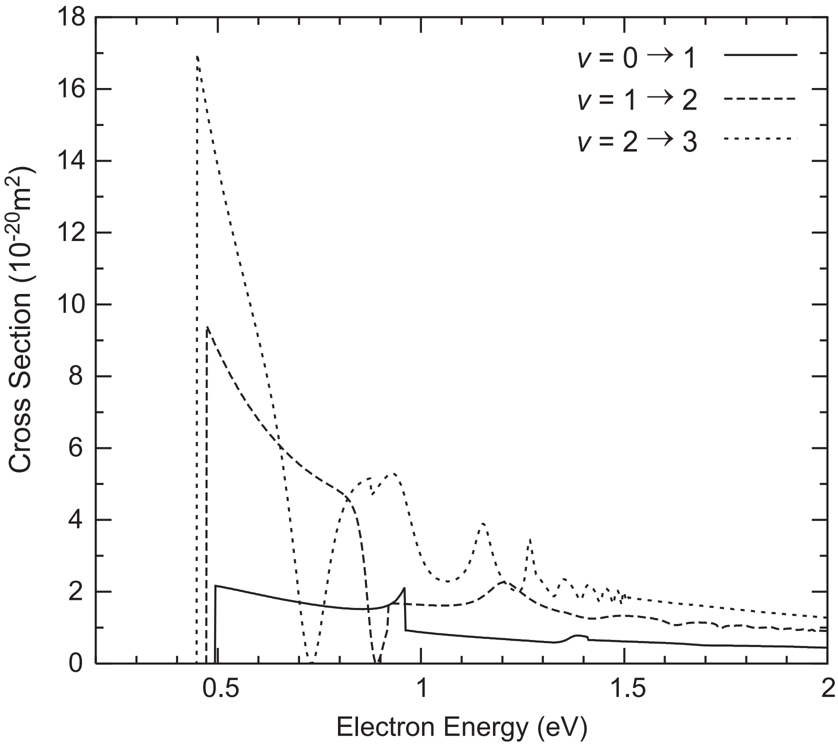

Figure 9. Calculated cross sections for excitation by one vibrational quantum.